

HIGH FIDELITY AIRWORTHINESS BIRD AND DRONE STRIKE ANALYSIS OF ON-DEMAND AIR MOBILITY SERVICE AIRCRAFT

Pradeep Vaghela¹, Hasan Raza¹, Eike Stumpf², and Javid Bayandor¹

¹CRashworthiness for Aerospace Structures and Hybrids (**CRASH**) Lab, Dept. of Mechanical and Aerospace Eng. University at Buffalo - The State University of New York, NY 14260, USA

²Institute for Aerospace Systems, RWTH Aachen University, NRW 52062, Germany

Abstract

Aircraft are prone to foreign object damage, especially bird strikes during take-off and landing. Modern air taxis are expected to make more frequent stops to serve as viable competition to the current urban transportation system. To ensure safety, it is important that any passenger aircraft meets crashworthiness regulations against foreign object damage such as bird strikes and drone impacts. With flying altitudes being below 10,000 *ft* and more frequent take-off and landing schedules, air taxis are particularly susceptible to such impacts. In this study, finite element methods are used to investigate the forces exerted by direct and oblique impacts on such an air mobility service vehicle. A bird surrogate, modeled using discrete particles, and a quadcopter drone were used as projectiles. Effects from debris ricochet were considered as part of impact analyses conducted. Dynamic forces from several bird and drone scenarios were analyzed and compared with each other to investigate the post-impact behavior of the aircraft.

Keywords: Air-taxi, Bird Strike, Drone Impact, Engine Ingestion, Foreign Object

1. Introduction

Traditional transportation modes are reaching their infrastructure and capacity limits, yet demand for transportation due to continual globalization is ever-growing. Similar to on-demand automobile transportation services, regional air mobility (RAM) services, also known as “On-Demand Air Mobility” (ODAM), could help alleviate problems related to the current transportation bottle-neck. Utilizing the third spatial dimension can effectively divert pressure from urban transportation infrastructure and reduce the traffic congestion associated with it [1]. Multiple companies are already working on the development of such ODAM services including e.SAT GmbH’s Silent Air Taxi, a piloted four-passenger aircraft featuring an innovative box-wing design with an electric drivetrain system [2-4].

Any air transportation mode is subject to foreign object impacts such as bird strikes during take-off and landing. Modern ODAM services that are under development would be required to make more frequent stops, making them further susceptible to such collisions. To ensure passenger safety, aircraft must meet the established crashworthiness regulations in the event of foreign object damage (FOD) [5,6]. Furthermore, with the advancement and increased usage of unmanned aircraft systems (UAS) such as drones, it becomes necessary to ensure the aircraft’s structural integrity in the event of a drone impact. There are certification guidelines from Federal Aviation Administration (FAA) developed based on extensive fuselage drop and bird strike trials. However, due to the high costs associated with such trials, it is impractical to conduct future certification studies purely through experimentation. Simulation methodologies in the meantime have advanced significantly in the past decade. Improvements in computational processing power are making simulations a more reliable and economic option for carrying out certification studies. Aerospace developers can now resort to computational approaches validated through representative physical trials to reduce the dependence on experimental tests. An example includes an assessment of a fuselage section crashworthiness through modeling. The computational approach used was partially validated by comparing the

simulation results with the drop test data conducted by FAA [7]. The reason for partial validation was the simplifications incorporated into the model to reduce the solution time. A complete validation of simulations will be possible in time pending the continued evolution of modeling capabilities and processing power. Presently, impact simulations can include validated, high fidelity, surrogate bird models to assist with certification efforts. Hence, detailed bird strike investigations were conducted for a new air-mobility type vehicle within the small aircraft category. To test the aircraft's capability to withstand other forms of FOD, caused by foreign objects with masses equal to those of the certification birds, drone impact simulations were also developed and run over the same aircraft parts (although not a required certification directive at this point). The study focused on the analysis of FOD due to direct or oblique impact by birds and drones. Impacts on the canopy, fuselage, and wings were considered for the modern ODAM platform selected with short take-off and landing (STOL) capabilities. The models were run on explicit finite element (FE) solver due to the high time dependency of the impact events. It should be emphasized that the modeled aircraft by no means included the structural details or was developed to represent the dynamic response of e.SAT to bird and drone strike events.

2. Numerical modeling

A detailed computer-aided model of the selected aircraft type was developed for the study. Figure 1 shows this representative CAD model which approximates the aircraft geometry. Typical values were chosen for several parameters and variables, otherwise not available in the open literature. LS-DYNA (LS-Dyna), a commercially available explicit FE code [8], with several user-defined measures added by the authors, were used to investigate the impact and post-impact behavior of the target components. Centered around certification mandates and due to their higher probability of FOD, canopy, wings, and fuselage structures were selected for impact scenarios. Advanced material models and techniques were incorporated into the simulations to describe the damage criteria, the onset of damage, failure modes, and progressive failure of the aircraft components. The total number of elements used in the FE simulation was 67,994 shells and 139,052 solid elements. Mesh quality was checked using parameters such as aspect ratio, warp angle, number of triangular elements, and skew. A summary is provided in Table 1.

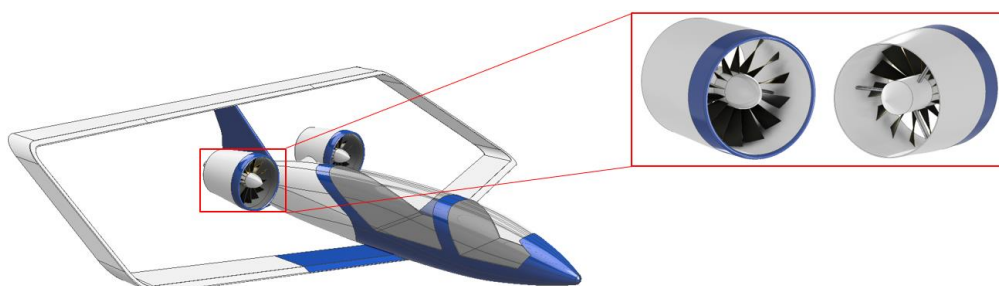


Figure 1 ODAM 3-D model showcasing the engines.

Table 1 Mesh quality parameters

| Parameter | Violation |
|--------------|------------------------|
| Aspect ratio | 1.89% (Allowable 10) |
| Warpage | 0.297% (Allowable 10) |
| Skew | 0.621% (Allowable 45°) |

2.1 Canopy

The canopy provides a safe cabin environment, minimizes aerodynamic drag, and acts as a protective barrier against wind and flying debris [9]. A dual canopy design was selected based on the general design of modern STOL aircraft. Such a design can provide effective stress distribution and dissipation between the canopies. Aircraft canopies are manufactured based on the flying altitude, velocity, and visibility required by the pilots/passengers. Figure 2 shows a dual canopy FE representation. For high impact resistance and optical transparency, polycarbonate was chosen as

the material for the canopies. The material properties were derived from an analysis performed on the F-16 [9,10]. The model has shell element formulations based on the Belytschko-Wong-Chiang section assignment if the hourglass energy stays under the permissible limit. For cases with higher hourglass energy, fully integrated Belytschko-Tsay [11] was used. It defines the element formulation, integration rules, nodal thickness, and cross-sectional properties of the FEM elements in the simulated environment. To attach the canopy to the fuselage, nodes were merged with the aligning nodes of the fuselage. The strength of the joint is limited by the failure strength of the weaker material in the merged nodes. The actual construction of the interface between the canopy to the fuselage will have additional structural elements. With the interface having higher failure criteria compared to the polycarbonate, special consideration should be taken to disregard failures close to the intersection. The simplification used to model the intersection reduced the computational time while sufficiently addressing the crashworthiness of the polycarbonate canopy structure for a direct bird or drone impact.

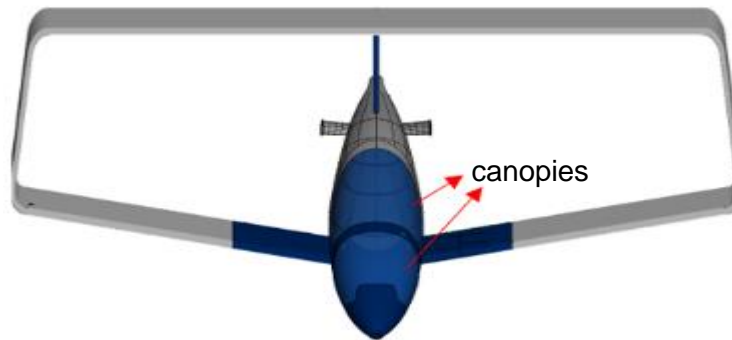


Figure 2 Discretized aircraft with canopies

2.1.1 Canopy material model

The elastic-plastic kinematic material model was selected with Cowper and Symonds strain hardening parameters [12,13]. The material is restrained by the proportionality limit within its elastic region, followed by the tangential modulus for the plastic region. Stresses in the plastic region were reported with the multiplication factor from Eq. (1) [8]. The material model and parameters were validated by a bird strike experiment performed by Brockman and Held [10]. The result of the simulations performed in this study provided consistency with [10] where the failure occurred at 350 *knots* bird impact velocity. This inspired confidence in the modeling scheme for the canopy.

$$\sigma_d = \sigma_s \left(1 + \frac{\varepsilon}{C}\right)^{\frac{1}{p}} \quad (1)$$

Where σ_d = dynamic yield stress, σ_s = static yield stress, ε = strain rate, and C and p are Cowper-Symonds constants.

2.2 Fuselage Structure and Wings

A lifting body fuselage was implemented for the aircraft model. Such a configuration, being considered for modern ODAM STOL aircraft, helps with increasing lift and reducing drag. Bulkheads and stringers were modeled as internal supports to provide structural integrity to the fuselage. Figure 3 shows the fuselage section of the model. Inspired by e.SAT, a box-wing design was developed for the model, for which light weight and high strength aerospace-grade aluminum alloy 606, commonly used in fuselage and wing structures of light aircraft, was selected.

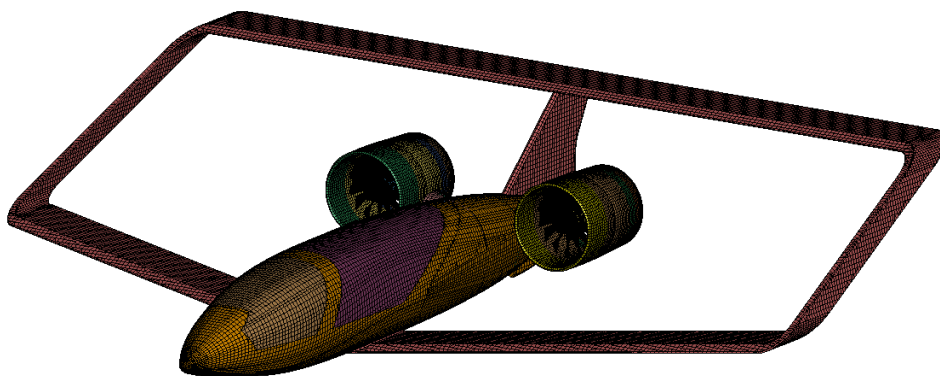


Figure 3 Meshed aircraft model

Internal structures were also implemented in the model near the proposed impact zone to provide structural integrity for the thin fuselage skin during impact. Without internal ribs and spars, the skin may incorrectly undergo large deformations. Figure 4 shows the internal structure of the model, inspired roughly by the structures seen in small aircraft. Estimated for the wing was also a wing box structure created to provide an internal reinforcement. In impact events, deformation and failure of the leading edge are the main areas of focus. Results from the preliminary simulations were used to guide the refinements of the internal fuselage and wing structures.

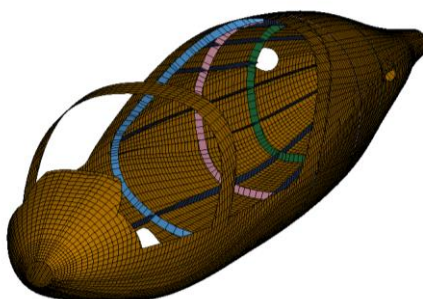


Figure 4 Fuselage and internal structures

2.3 Impactor Models

For modeling the bird surrogate the Smoothed Particle Hydrodynamics (SPH) technique was used. This was since SPH is more versatile and can capture large structural deformations more effectively than other available methods requiring complex mesh. Mesh entanglement issues seen in other methods due to large deformations can also be avoided if a particle method is used. As a result, the particular SPH element formulation used for the bird model allowed for precise particle tracking throughout the impact window without encountering numerical errors.

An equal mass drone model was also developed in compliance with the FAA 14 CFR Part 107 directive, which indicates that a drone of 55 *lb* (24.95 *kg*) or less can be used [14]. It has been shown extensively by Bayandor and team [5-9] since 2015 that even drones within mass ranges similar to those of the certification birds for small and large piloted aircraft can pose grave collision and damage threats to their respective aircraft platform.

2.3.1 Bird Modeling

A bird strike on aircraft is classified as a soft impact event. Soft impact occurs when the projectile has a much lower strength than the target, causing extensive deformation of the projectile over the target surface [15–20]. The large and fluidic distortions seen in bird strikes demand the application of the theory of hydrodynamics for the modeling of corresponding scenarios. High pressure waves are generated as part of high-velocity impacts. Therefore, the equation of state (EOS) utilized for an SPH solution needs to use hydrodynamic pressure-volume relations to describe the high pressure fronts created by the soft impact. Several equations have been used in the past bird impact studies [21–28]. However, no common agreement appears to exist on which EOS is most appropriate for bird impact modeling. Typically, in all different forms of EOS, the methodology is to substitute water material

HIGH FIDELITY DRONE AND BIRD STRIKE ANALYSIS ON ODAM

properties for the bird and calibrate the state equation values until the desired peak pressure or impact pressure-time history profile is observed similar to the experimental results reported by Wilbeck [15,29]. Equation (2) shows the expression for the shock pressure, or Hugoniot pressure that is generated inside of a surrogate bird model upon impact, assuming both the impactor and target behave elastically.

$$P_H = P_2 - P_1 = \rho_o U_s U_o \quad (2)$$

Where, ρ_o is the bird density before impact, U_o is the relative impact velocity and U_s is shock velocity, defined using Eq. (3):

$$U_s = c_o + kU_o \quad (3)$$

c_o is the speed of sound in the undisturbed object (before the impact) and k is a material compressibility coefficient. As the impact initiates the fluid-structure interaction (transition of the solid bird into fluidic bulk), the pressure release waves force the fluidic material away from the center of the projectile and out of its control volume. The shock pressure decays to a lower steady pressure [14,25], derived from Eq. (4):

$$P_s = \frac{1}{2} \rho_o U_o^2 \quad (4)$$

In this study, a linear polynomial EOS was used. To comply with current standard practices for bird modeling, a cylindrical volume with hemispherical caps was considered to approximate the bird geometry. FAA 14 CFR § 23.2320(b) [30] requires the canopy of a Level 4 aircraft (Level 4 - for aircraft with a maximum seating configuration of 10 to 19 passengers) to withstand impact without penetration from a 2 lb (900 g) bird. Considering this requirement, a bird mass of 900 g (2 lb) was chosen to constitute a large pigeon size surrogate. Figure 5 shows the dimensions of the SPH bird model developed.

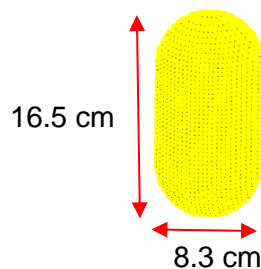


Figure 5 Cylindrical SPH bird impact model.

A length to width ratio of 2 was chosen with a total number of particles to be approximately around 17,500. The density of the bird was kept to 950 kg/m^3 , which is water density with 10% air added to represent porosity. Table 2 summarizes the key modeling parameters applied.

Table 2 Bird modeling parameters

| Parameter | Value |
|----------------------|----------------------|
| Density, ρ | 950 kg/m^3 |
| Compressibility, k | 2 |
| Speed of sound, c | 1482.5 m/s |
| Bulk modulus, K | 2.05 GPa |

2.3.2 Drone Modeling

The drone model was developed to match the mass and size of the bird surrogate. As indicated, birds are considered soft body objects with fluidic behavior during impact. Drones have solid structures that do not behave like fluid at contact. At impact, drones can fragment into pieces with high density which can further cause damage to other crucial parts of the aircraft on rebound. In the model, the battery was assigned lithium polymer properties and was positioned inside the main body of the drone. Various electronic components with a range of material properties similar to circuit boards were also included in the model. An estimate of copper and plastic material properties were used for the motors. The propellers and center hub were considered to be made of carbon fiber composite and aluminum 6061, respectively. The main body and the four struts were modeled as acrylonitrile butadiene styrene (ABS). The elastic-plastic material model was used to model ABS and aluminum, and an enhanced composite damage model for the carbon fiber composites. The detailed impact model of the quad-rotor UAS developed is displayed in Figure 6. Table 3, and Tables 4 and 5 provide the details of the drone model components and material considerations, respectively.

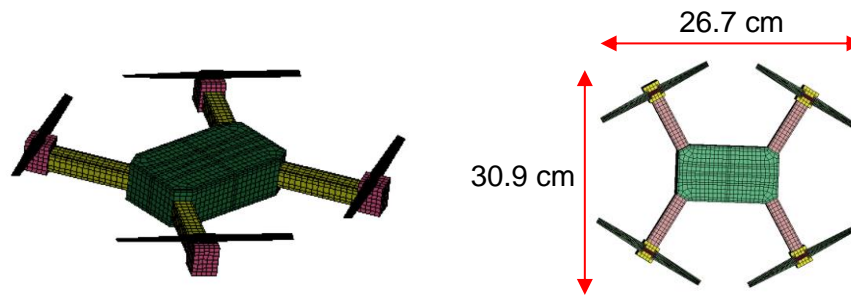


Figure 6 Drone impact model with an equivalent mass to the surrogate bird

Table 3 Mass distribution of the drone

| Component | Material | Mass (Kg) |
|------------------|--------------------|-----------|
| Propeller | Carbon fiber | 0.0132258 |
| Battery | Li- Polymer | 0.4849600 |
| Main frame, Arms | ABS | 0.0981550 |
| Powerplant | Copper and polymer | 0.1745290 |
| Internal Parts | Circuit board | 0.0865871 |
| Total mass | | 0.9308190 |

Table 4 Properties of different materials used in the drone model [31–33]

| | Elastic Modulus (Pa) | Yield Stress (Pa) | Tangential modulus (Pa) | Poisson's ratio | Density* (kg/m ³) | Failure Strain |
|--|------------------------|--------------------|-------------------------|-----------------|-------------------------------|----------------|
| ABS | 2.082×10^8 | 3.99×10^7 | 9.653×10^6 | 0.300 | 1774 | 0.02 |
| Li-Polymer | 5×10^8 | 3×10^7 | 5×10^7 | 0.300 | 1440 | 0.02 |
| Powerplant | 1.182×10^{11} | 3.33×10^7 | 1.760×10^8 | 0.343 | 1403 | 0.10 |
| <i>* Density values are modified in the simulation to adjust the mass of the drone</i> | | | | | | |

Table 5 Carbon fiber material property

| Property | Density (kg/m ³) | Elastic modulus A (Pa) | Elastic modulus B/C (Pa) | Poisson's ratio A/B/C | Shear modulus A/B (Pa) | Shear modulus C (Pa) |
|------------|------------------------------|------------------------|--------------------------|-----------------------|------------------------|----------------------|
| Value (SI) | 1780 | 1.57×10^{11} | 8.5×10^9 | 0.0189 | 4.40×10^9 | 3.2×10^9 |

3. Impact Scenarios

Impact locations selected as part of the present study included canopy, fuselage, and wings due to the high probability of contact with a foreign object [5,8]. The impact scenario concerning the canopy was selected based on the FAA certification requirements for bird size and impact velocity for small aircraft, which for Level 4 aircraft demands that each canopy and its supporting structure directly in front of the pilot must withstand, without penetration, the impact equivalent to a two-pound bird when the velocity of the airplane is equal to the airplane's maximum approach flap speed [30]. The impact velocity was set to 81 *m/s*, which corresponds to the approach speeds defined through 14 CFR Part 23 for small aircraft [30]. For consistency, drone impact was performed at the same velocity. The drone model was tilted forward by 25° based on the maximum tilt angle for similar size physical drones.

3.1 Canopy Impact

In small aircraft, the canopy will be the first part to come into contact with any foreign objects approaching the cockpit, therefore a critical component to be tested to ensure crashworthiness. Bird and drone impact scenarios are shown in Figs. 7 and 8 at their initial contact time as well as the time for their peak deformation. For the bird impact, the structural stresses did not exceed the yield stress. In the drone scenario, the canopy was plastically deformed. Within the drone simulation, stresses for several elements almost reached those of the failure criteria, making the canopy susceptible to crack initiation and propagation at the location of these elements. For the bird scenario, the canopy did not show any severe sign of failure.

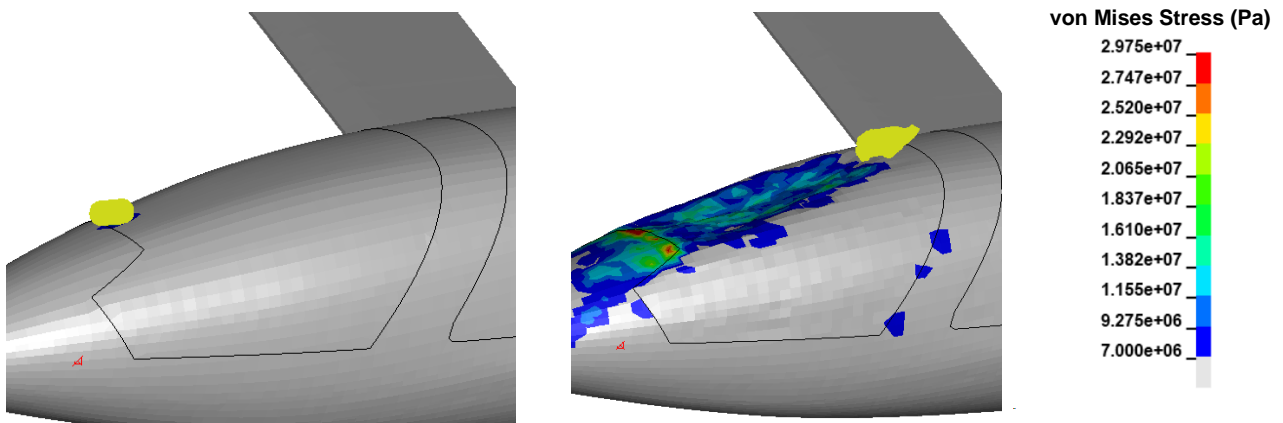


Figure 7 Bird impact on the canopy

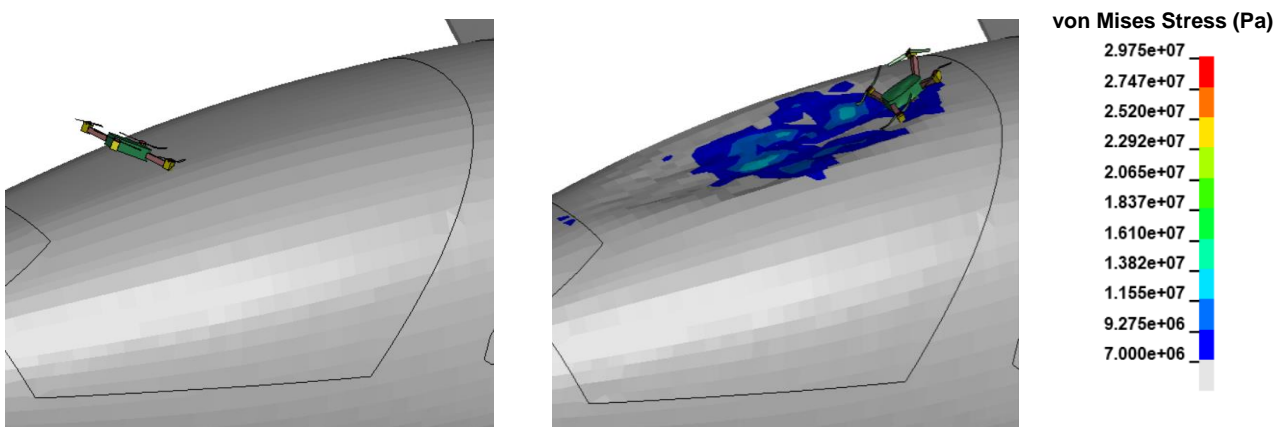


Figure 8 Drone impact on the canopy

3.2 Fuselage Impact

Bird strike perpendicular to the fuselage is not a likely scenario. The maximum relative velocity of the bird-aircraft is close to the approach speed of the aircraft. Hence, based on the vector projection, the impact angle of 45° against the aircraft fuselage can be considered. The outer thin metal layer of the fuselage was observed for any deformation caused by impact. The fuselage skin was reinforced with a non-design-specific series of ribs and spars to provide required strength. After completing the simulation runs, the results revealed various stress concentration points. Bird and drone post impact turn into debris and the possibility of hitting other parts or being ingested by the engine remains. Engine ingestion effects are not considered in this study. Water like nature of the bird SPH elements distributes the impact force over a large surface area of the fuselage. Lagrangian elements with higher density concentrate the force on the impact zone. Figures 9 and 10 show the von Mises stresses induced by bird and drone impact on the fuselage. The severity of damage caused by drone impacts is higher due to the high force and, hence, stress concentrations over the impact zone. Similar to impacts onto the canopy though, bird strikes result in the formation of wider spread stress profiles on and around the impact region on the fuselage.

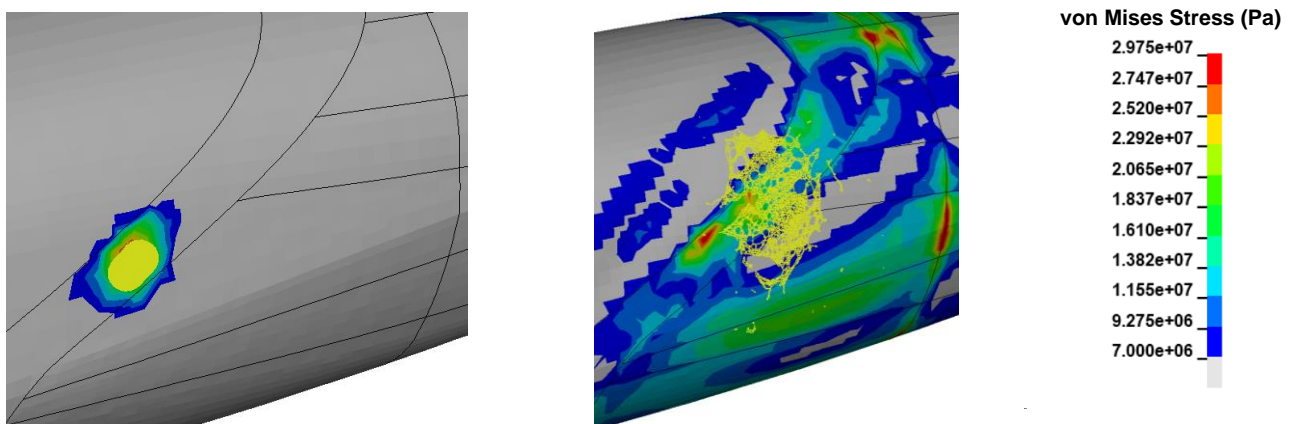


Figure 9 Bird impact on the fuselage

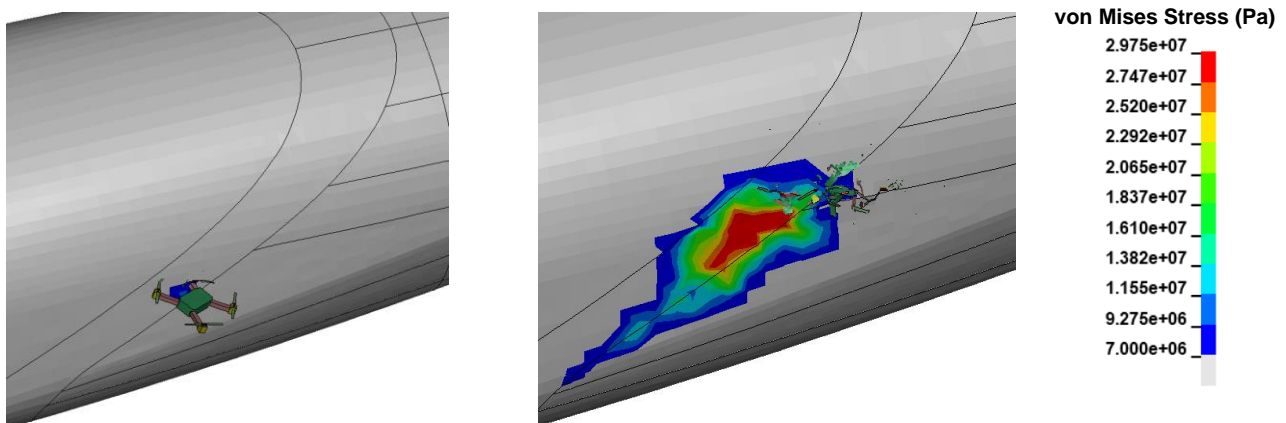


Figure 10 Drone impact on the fuselage

3.3 Wing Impact

Figures 11 and 12 show the bird and drone impacts on the leading edge of the wing. The fringe limit is changed to a different range to better visualize the stress level. Note that the stress distribution over the structure is significantly less compared to the bird impact. Similar to the earlier cases, soft bird material particles distribute the force over a larger surface area. Drone fragments with higher density do not spread and result in creating high pressure points over the impact zone. This causes a more drastic wing leading edge deformation compared to that resulting from the bird impact.

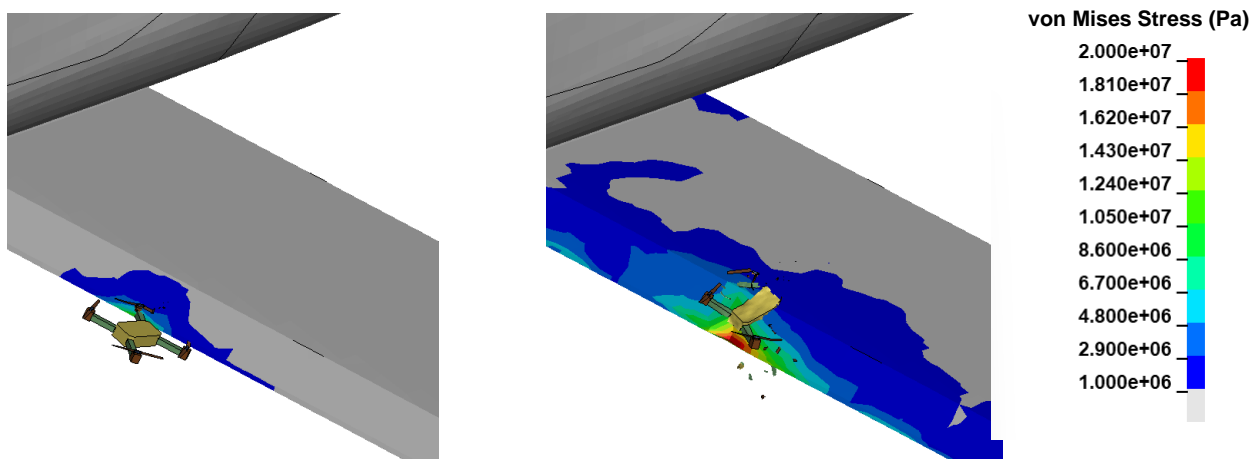


Figure 11 Drone impact on the wing

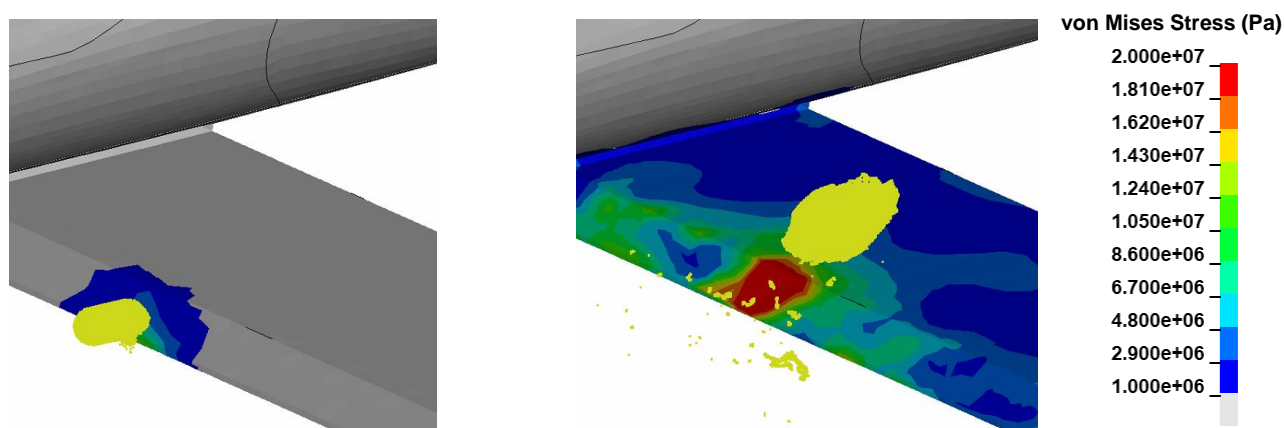


Figure 12 Bird impact on the wing

4. Impact Results

To get a better appreciation of the analyses shown in Figs. 7 to 12, reaction forces, deformation, and energy for each case were assessed. Reaction forces are indicative of impact force applied to the aircraft. Force values from FEA can have an unsteady response due to the setups of contact algorithms and/or the proximity of the projectile nodes with the target nodes. The instantaneous force may therefore not be accurately captured. Consequently, data filtering using moving mean value is used in the force-time history plots to provide a closer physical representation. The moving mean method takes an average of a number of points within a close time range, and subsequently filters the results and removes numerical noise by eliminating overly high or low peaks. Energy-time history shows whether any hourglass effects (zero-energy modes of deformation that produce zero strain and no stress), are occurring. To avoid hourglassing, in most cases a fully integrated element formulation was used. This can be observed in energy plots where hourglass energy stays at zero. Deflection plots show the 2-D cross-sectional view of the individual parts superimposed at the impact location to better visualize the deformation caused by the impacts.

4.1 Canopy Impact

Figure 13 shows the force-time history plot for the windshield impact scenario. The force values for the bird and drone are significantly different, however the deflection of the canopy due to the bird and drone impacts is similar. In the deflection plot, deformation of the canopy at 6 ms is shown. At 12 ms after initial impact, the deformation is nearly identical for the bird and drone. Figure 14 includes the energy plot for the windshield. As the impact occurs, the internal energy rises with the kinetic energy. This is due to the fact that the windshield moves and deforms, influencing both energy levels. The internal and kinetic energies interchange within the windshield as the component deforms and finds another plastically deformed, yet stable, state before the deformation stops.

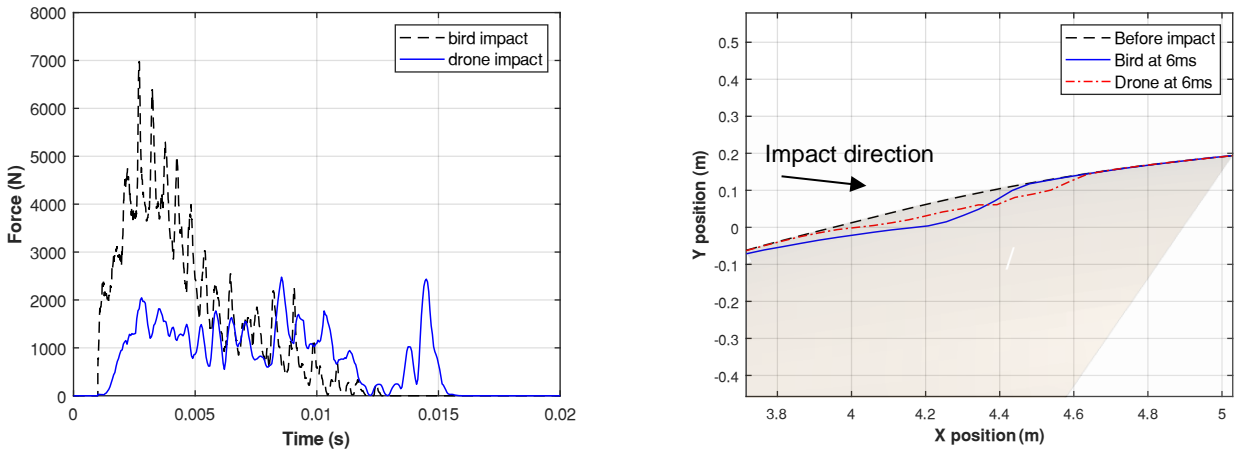


Figure 13 Force vs time comparison between bird and drone impacts on the canopy and, deflection plot

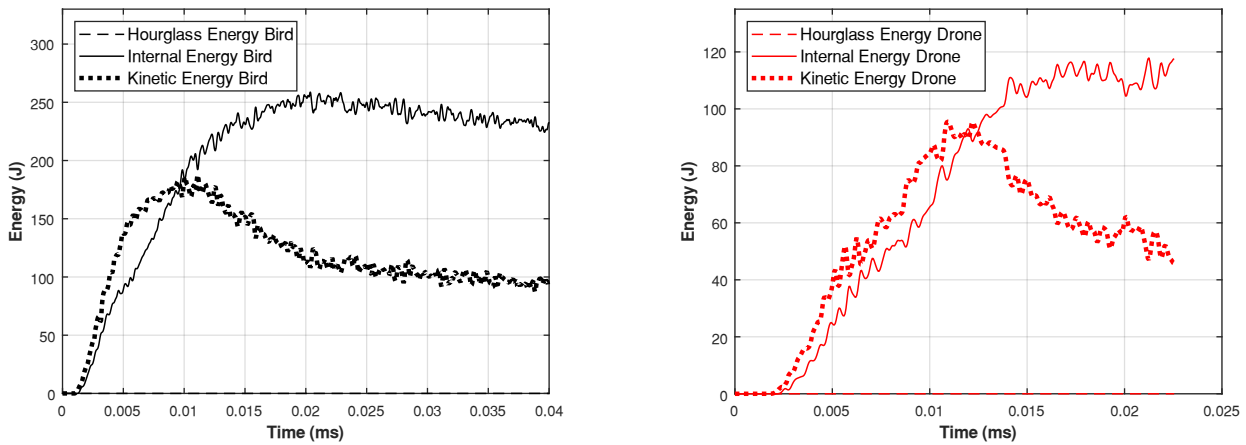


Figure 14 Energy-time history for bird and drone impacts on the canopy

4.2 Fuselage Impact

Figure 15 captures the deflection plot not showing any significant deformation, which is indicative of the high strength of the fuselage. Force values for the bird strike in Figure 15 follow the same pattern as those of the windshield impact. For drone, the forces are distributed over larger impact window compared to those of the bird. Energy transfer for the fuselage impact can be seen in Figure 16. For the bird impact on the fuselage, efficient element formulation with fewer integration points was used. This method reduced any hourglass effects, limiting the hourglass energy to less than 10% of the total energy, an acceptable value for impact simulations [13].

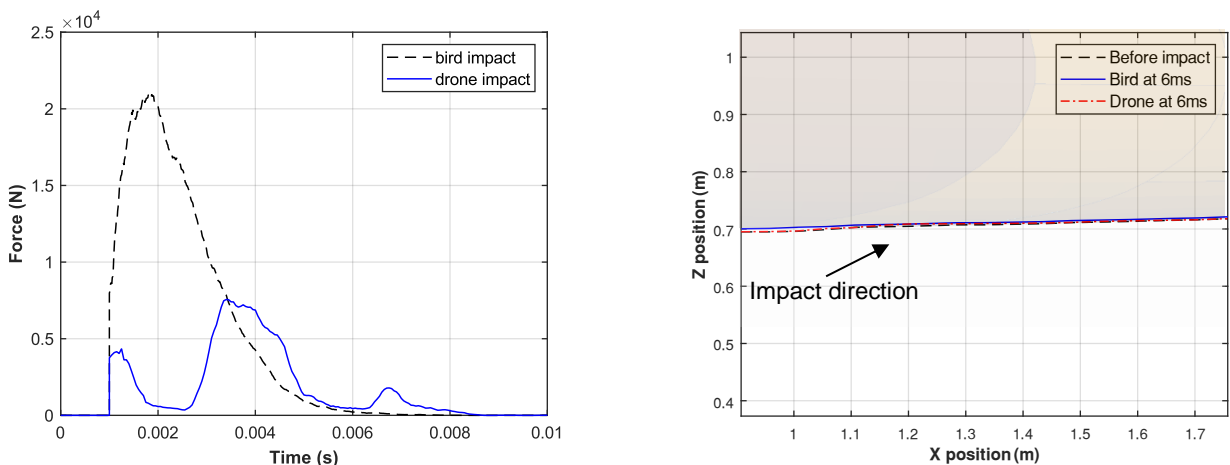


Figure 15 Force-time history and deflection plots for the bird and drone impact

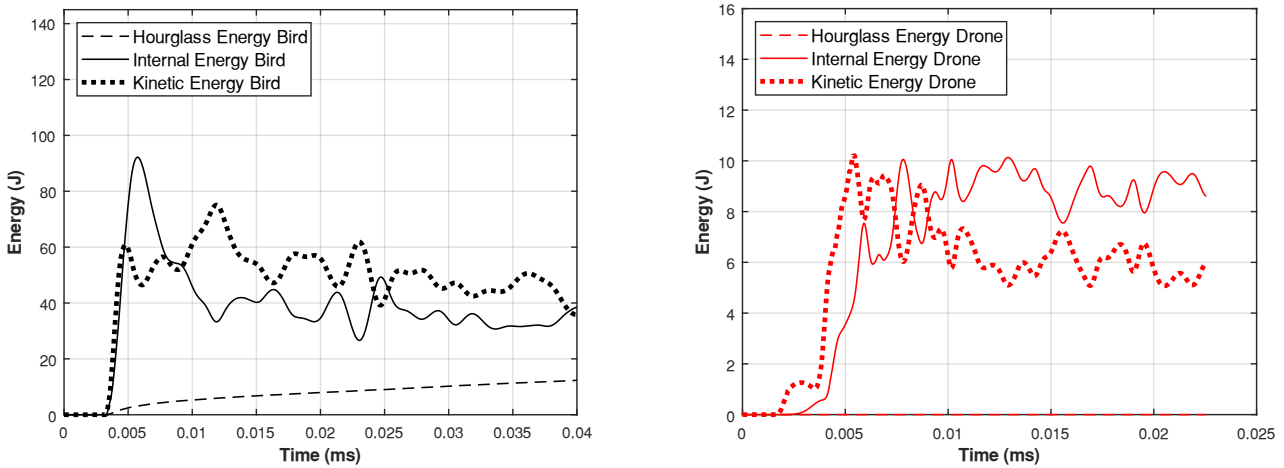


Figure 16 Energy-time history for bird and drone impacts on the fuselage

4.3 Wing Impact

Wing impact force and energy plots follow the same trend as the earlier impact scenarios. The deflection plot for the leading edge of the wing shows a significant deformation for the drone impact case only. Furthermore, the average deflection is considerably higher in the drone scenario. Force values do not align well with the deflection values for the drone impact. The considerably higher deflection from the drone impact is likely the result of its solid structural components such as the batteries, powerplant, and the mainframe. However, force-time history results show lower impact force than the bird strike. This is since the drone components are eroded (deleted) from the computational domain once they reach failure criteria, and their masses removed from the simulation. Therefore, an overall lower reaction force is registered by the FEA as part of the drone impact event. Figure 17 displays the force values, and deflection at 6 ms after the initial contact. The energy plot is captured by in Figure 18.

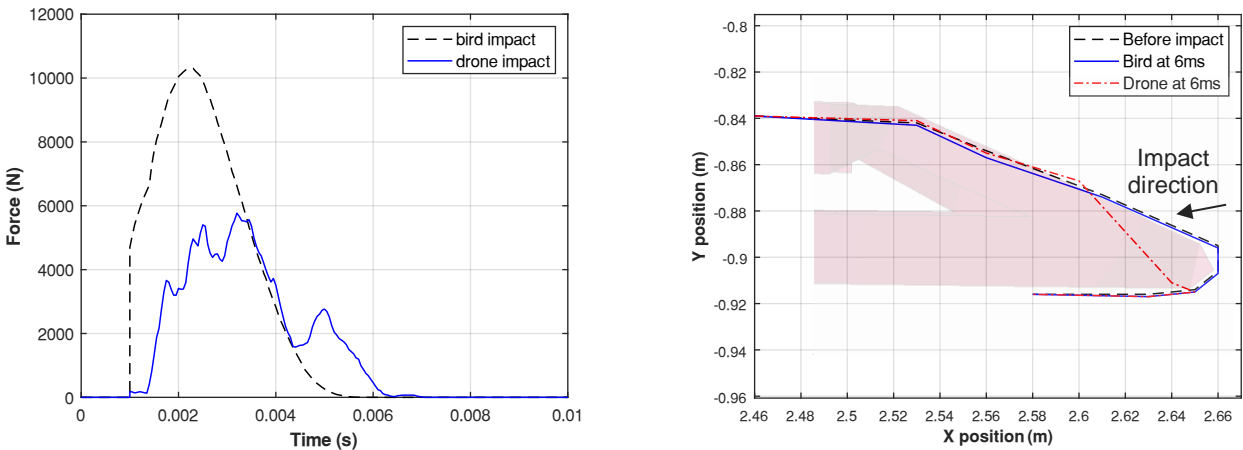


Figure 17 Force-time history and deflection plots for the bird and drone impact

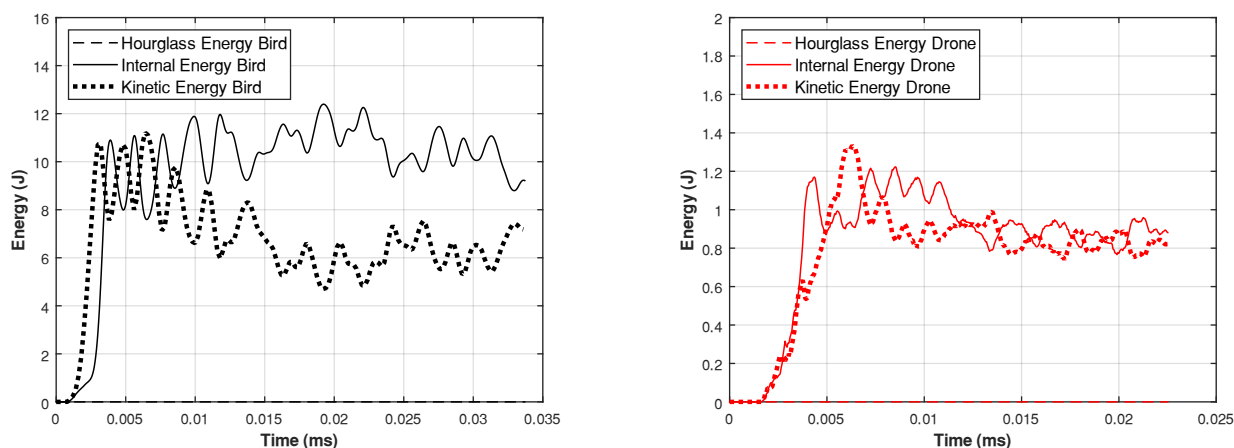


Figure 18 Energy-time history for bird and drone impacts on the fuselage

5. Conclusion

For the collision cases considered as part of the crashworthiness research reported here, bird strike produced higher force values with higher stress distribution over the structure. This was due to the reaction forces from individual bird particles accruing throughout the impact process. For the drone impact however, this was not the case as the elements from the drone components that reached the set failure criteria were removed from the computational domain and thereby did not further intensify the force-time history. The force value is plotted for the entire wing, fuselage, and windshield's accrued reaction force caused by the projectile. The deformation is larger or the same in all impact scenarios for the drone case compared to that of the bird, due to the fact that the bird surrogate was modeled as a soft body with fluidic behavior on impact. The drone components on the other hand failed to solid fragments, which generally resulted in larger deformations.

The drone model in this study was not designed for elastic deformation, as it was considered to be predominantly made of hard and brittle plastic (with no metallic chassis), which could undergo failure at relatively low strains. Therefore, at failure, these elements absorbed some of the impact energy, causing the drone impact peak force to drop as the parts coming into contact with the target were fragmented. The fluidic nature of the SPH bird allows the force to be distributed over a larger area, which creates a pressure point on the surface of the aircraft at the impact zone. Subsequently, the high pressure generated causes the deformation, and not failure, of the thin aircraft aluminum skin as shown by the simulations. There is a difference in deletion algorithms between SPH and Lagrange element formulations. The SPH nodes remain in the FEA environment after the failure criteria (pressure cut-off) is reached, and proceed to hit the structure, which then gives rise to the large stresses and reaction forces. When undergoing failure, the failed drone elements however are no longer included in the calculations and deleted. Their deletion from the domain also has the potential to remove their masses from the simulation. If the eroded masses are not intentionally added back to the remaining nodes, the projectile cannot cause any further damage to the target after the initial collision. In real-life scenarios, after fragmentation, the drone pieces and debris will cause a similar effect as SPH. There are ways to reintroduce the deleted mass back into the simulation. For the windshield, a perpendicular hit might cause more damage, but it is not possible for the drone to collide with an airborne aircraft at the right angle at its relative velocity. Hence, a feasible, yet critical, scenario was chosen for the windshield. Considering the above, it was shown that the drone caused similar to more damage to the target compared to the surrogate bird. Therefore, for the same mass category and based on a series of high-fidelity simulations, it is apparent that drone impact events can lead to more consequential damage and that future aircraft design procedures should be informed by this new foreign object threat.

6. Contact Author Email Address

Corresponding author:

Javid Bayandor; bayandor@buffalo.edu

7. Copyright Statement

The authors confirm that they, and/or their company or organization, hold copyright on all of the original material included in this paper. The authors also confirm that they have obtained permission, from the copyright holder of any third party material included in this paper, to publish it as part of their paper. The authors confirm that they give permission, or have obtained permission from the copyright holder of this paper, for the publication and distribution of this paper as part of the ICAS proceedings or as individual off-prints from the proceedings.

8. Acknowledgments

The authors would like to highly acknowledge RWTH Aachen, the Theodore von Karman Fellows Committee, and e.SAT for their sponsorship of this project. RWTH Aachen's Institute for Aerospace System and e.SAT's invitation to join the crashworthiness investigations is further greatly acknowledged. Special thanks go to CRASH Lab team, particularly Matthew Thornton and Nicholas Noviasky for their input and important contribution to the project.

References

- [1] Schuh G, Spangenberg M and Freitag M. Assessment of Top Level Specifications For Urban and Regional Air Mobility Vehicles. *Deutsche Gesellschaft für Luft-und Raumfahrt-Lilienthal-Oberth eV*, pp 1–9, 2021.
- [2] Uber. UBER Elevate. [Online]. Available at: <https://www.uber.com/us/en/elevate/>. [Accessed: 07-Feb-2022].
- [3] AIRBUS. CityAirbus NextGen. [Online]. Available at: <https://www.airbus.com/en/innovation/zero-emission/urban-air-mobility/cityairbus-nextgen>. [Accessed: 02-Jul-2022].
- [4] Stumpf E., Kreimeier M., Strathoff P., Lückhof J., Schröder K. U. and Janser F. Small aircraft concept for regional on-demand air mobility. *31st Congress of the International Council of the Aeronautical Sciences*, Belo Horizonte, Brazil, 2018.
- [5] Song Y., Horton B. and Bayandor J. Investigation of UAS ingestion into high-bypass engines, Part 1: Bird vs. Drone, *58th AIAA/ASCE/AHS/ASC Structures, Structural Dynamics, and Materials Conference*, Grapevine, Texas, USA, 2017.
- [6] Schroeder K., Song Y., Horton B. and Bayandor J. Investigation of UAS Ingestion into High-Bypass Engines, Part 2: Parametric Drone Study, *58th AIAA/ASCE/AHS/ASC Structures, Structural Dynamics, and Materials Conference*, Grapevine, Texas, USA, 2017.
- [7] Megharaja S. J. and Bayandor J. Comprehensive Analysis of Fluid-Structure Interactive Schemes for Modeling Aircraft Water Impact Scenarios, *Proceedings of Fluids Engineering Division Summer Meeting (FEDSM)*, 2020.
- [8] Livermore Software Technology Corporation (LSTC), LS-DYNA user manuals. Livermore, CA, USA, 2020.
- [9] Siddens A. J., Bayandor J. and Abdi F. Soft impact damage prognosis of F-16 canopy using progressive failure dynamic analysis. *Journal of Aircraft*. Vol. 51, No. 6, pp 1959–1965, 2014.
- [10] Brockman R. A. and Held T. W. Explicit Finite Element Method for Transparency Impact -Analysis, WL-TR-91-3006, Dayton University Research Insitue, 1991.
- [11] Belytschko T, Lin J I and Chen-Shyh T. Explicit algorithms for the nonlinear dynamics of shells. *Computer Methods in Applied Mechanics and Engineering*, Vol. 42, No. 2, pp 225–251, 1984.
- [12] Cowper, G. R. and Symonds, P. S. Strain-hardening and strain-rate effects in the impact loading of cantilever beams. Brown University, Providence, RI, USA, 1957.
- [13] Foster M., Love B., Kaste R. and Moy P. The Rate Dependent Tensile Response of Polycarbonate and Poly-methylmethacrylate. *Journal of Dynamic Behavior of Materials*. Vol. 1, No. 2, pp 162–175, 2015.
- [14] FAA. Small Airplanes Regulations, Policies & Guidance, Aircraft Certification. [Online]. Available at: https://www.faa.gov/aircraft/air_cert/design_approvals/small_airplanes/small_airplanes_regs/.
- [15] Siddens A. and Bayandor J. Multidisciplinary impact damage prognosis methodology for hybrid structural propulsion systems. *Computers and Structures*. Vol. 122, pp 178–191, 2013.
- [16] Kim M., Zammit A., Siddens A. and Bayandor J. An Extensive crashworthiness methodology for advanced propulsion systems, Part I: Soft impact damage assessment of composite fan stage assemblies. *49th AIAA Aerospace Sciences Meeting Including the New Horizons Forum and Aerospace Exposition*, Orlando, Florida, USA, 2011.
- [17] Zammit A., Kim M. and Bayandor J. Bird-strike damage tolerance analysis of composite turbofan engines. *27th Congress of the International Council of the Aeronautical Sciences*, Nice, France, 2010.

HIGH FIDELITY DRONE AND BIRD STRIKE ANALYSIS ON ODAM

- [18] Bayandor J., Johnson A. F., Thomson R. and Joosten M. Impact Damage Modelling of Composite Aerospace Structures Subject to Bird-Strike, *25th Congress of the International Council of the Aeronautical Sciences*, Hamburg, Germany, 2006.
- [19] Joosten M. and Bayandor J. Coupled SPH-composite cohesive damage modeling methodology for analysis of solid-fluid interaction, *46th AIAA Aerospace Sciences Meeting and Exhibit*, Reno, Nevada, USA, 2008.
- [20] Wilbeck J. S. Development of a Substitute Bird Model. *Journal of Engineering for Power*. Vol. 103, No. 4, pp 725–730, 1981.
- [21] Siddens A. and Bayandor J. Multidisciplinary impact damage prognosis methodology for hybrid structural propulsion systems. *Computers and Structures*. Vol. 122, pp 178–191, 2013.
- [22] Vignjevic R., Orłowski M., De Vuyst T. and Campbell J. C. A parametric study of bird strike on engine blades. *International Journal of Impact Engineering*. Vol. 60, pp 44–57, 2013.
- [23] Liu J., Li Y. and Gao X. Bird strike on a flat plate: Experiments and numerical simulations. *International Journal of Impact Engineering*. Vol. 70, pp 21–37, 2014.
- [24] McCarthy M. A., Xiao J. R., McCarthy C. T., Kamoulakos, A., Ramos, J., Gallard, J. P. and Melito, V. Modelling of bird strike on an aircraft wing leading edge made from fibre metal laminates - Part 2: Modelling of impact with SPH bird model. *Applied Composite Materials*. Vol. 11, No. 5, pp 317–340, 2004.
- [25] Moffat T. J. and Cleghorn W. L. Prediction of bird impact pressures and damage using MSC/DYTRAN. *Proceedings of the ASME Turbo Expo*. Vol. 4, pp 1–9, 2001.
- [26] Lavoie M. A., Gakwaya A., Ensan M. N., Zimcik D. G. and Nandlall D. Bird's substitute tests results and evaluation of available numerical methods. *International Journal of Impact Engineering*. Vol. 36, No. 10–11, pp 1276–1287, 2009.
- [27] Allaëys F., Luyckx G., Van Paepegem W. and Degrieck J. Numerical and experimental investigation of the shock and steady state pressures in the bird material during bird strike. *International Journal of Impact Engineering*. Vol. 107, pp 12–22, 2017.
- [28] Siddens A. and Bayandor J. Soft impact assessment methodology for hybrid structure aerospace engines. *50th AIAA Aerospace Sciences Meeting Including the New Horizons Forum and Aerospace Exposition*, Nashville, Tennessee, USA, 2012.
- [29] Wilbeck J. Impact Behaviour Of Low Strength Projectiles. *Air Force Materials Laboratory*, 1977.
- [30] FAA. Code of Federal Regulations : PART 23-AIRWORTHINESS STANDARDS: NORMAL CATEGORY AIRPLANES. *Title 14 Code of Federal Regulations (14 CFR)*, [Online]. Available at: <https://www.ecfr.gov/cgi-bin/textidx?SID=685dc1ae97ae3f5e5569e47880fab01e&mc=true&node=pt14.1.23>, 2021.
- [31] Joy J, Winkler K, Joseph K, Anas S and Thomas S. Epoxy/methyl methacrylate acrylonitrile butadiene styrene (MABS) copolymer blends: Reaction-induced viscoelastic phase separation, morphology development and mechanical properties. *New Journal of Chemistry*, Vol. 43, No. 23, pp 9216–9225, 2019.
- [32] Christiyan K. G. J., Chandrasekhar U. and Venkateswarlu K. A study on the influence of process parameters on the Mechanical Properties of 3D printed ABS composite. *IOP Conference Series: Materials Science and Engineering*. Vol. 114, No. 1, 2016.
- [33] Ahn S. H., Montero M., Odell D., Roundy S. and Wright P. K. Anisotropic material properties of fused deposition modeling ABS. *Rapid Prototyping Journal*. Vol. 8, No. 4, pp 248–257, 2002.